Pergamon

Acta Astronautica Vol. 32, No. 5, pp. 363–376, 1994

0094-5765/94 $7.00 + 0.00

SATELLITE NAVIGATION FOR METEOROLOGICAL PURPOSES: INVERSE REFERENCING FOR NOAA-N AND ERS-1 IMAGERS WITH A 1 km NADIR PIXEL SIZE†

J. KLOKOČNÍK,[1] J. KOSTELECKÝ,[2] H. GRASSL,[3,4] P. SCHLÜSSEL,[4] L. POSPÍŠILOVÁ,[1] R. H. GOODING[5] and P. LÁLA[6]

[1]Astronomical Institute, Czech Academy of Sciences, CZ-251 65 Ondřejov Observatory, Czech Republic, [2]Research Institute for Geodesy, CZ-250 66 Zdiby 98, Czech Republic, [3]Max Planck Institute for Meteorology, Bundesstrasse 55, D-2000 Hamburg 13, Germany, [4]Meteorological Institute, University of Hamburg, Bundesstrasse 55, D-2000 Hamburg 13, Germany, [5]Defence Research Agency, Aerospace Division, Farnborough GU14 6TD, England and [6]Outer Space Affairs Division, U.N. Secretariat, Room S-3270A, New York, NY 10017, U.S.A.

(Received 12 May 1993; received for publication 13 October 1993)

Abstract—Iterative methods for inverse referencing from mean orbital elements or osculating position and velocity, accounting for all necessary orbital perturbations with respect to given nadir pixel size, are described. [Inverse referencing means that the geodetic coordinates of a point on the surface are given and the corresponding image coordinates (scan line number and pixel number) are obtained from satellite orbital elements or coordinates.] The idea is to treat a pixel like a satellite tracking station on the ground. This permits the use of existing software for the computation of satellite ephemerides and orbit determination. The time of culmination of a satellite over the pixel and the off-nadir angle at that moment have been computed. Two variants for such a computation have been tested. Numerical results for the NOAA-N meteorological satellites and ERS-1 are presented. The present state of our software for inverse referencing should fulfil ordinary requirements posed by meteorologists. For NOAA-N satellites, the accuracy achieved roughly the nadir pixel size. The main obstacle to an increase in accuracy is the low quality of the mean orbital elements usually available. For ERS-1, the accuracy may achieve a level of 100 m. A software package, containing versions of the FORTRAN 77 programs PIXPO 3, PIXPO 4 and PIXPOSC, for various data types, including US-2 line or TBUS mean elements or a state vector, is available for scientific exchange.

1. OUTLINE

If satellite image data are used for trend analysis, description of the annual course, climatic mean values etc., then satellite pixel navigation might become an important error source. In order to reduce this error source we have tried to compile a software package taking into account the usually low quality of orbital elements, restricting the computer code to main forces acting on a satellite, and keeping in mind the restricted computer capacity.

This paper deals with navigation for radiometer experiments on low-flying, nearly-polar, nearly-circular orbits of NOAA-N meteorological satellites and the remote-sensing satellite ERS-1. The "navigation" can be understood as an application of the orbit prediction and determination process, whereby the accuracy requirements are moderate, corresponding to nadir pixel size of order 1 km^2, in contrast to the strict demands of geodesy, altimetry and geodynamics.

In satellite navigation (see, for example, Ho and Asem [1] or Emery *et al.* [2]) *direct* and *inverse referencing* are distinguished. The former is to locate a subsatellite point or a pixel of an image by assigning a scan line l and a pixel number p for a given time, from mean orbital elements of the particular epoch, i.e. to find geodetic (geographic) coordinates of that point. Inverse referencing means that the geodetic coordinates of a place of interest (projection of pixel on a surface, or Ground Control Point, GCP) are given and we seek the corresponding image coordinates (l, p), using the mean orbital elements at an epoch (or the state vector, i.e. $X, Y, Z, \dot{X}, \dot{Y}, \dot{Z}$) of the satellite. The flow of information from the orbital data to the time of culmination and the off-nadir angle, which are simply related to the pixel indices (l, p), is indicated in Fig. 1.

During the direct or inverse referencing, the orbital effects of various disturbing accelerations arising from gravitational and non-gravitational sources must be included. The most important effect is from

†Paper IAF-92-57 presented at the *43rd Congress of the International Astronautical Federation*, Washington, D.C., U.S.A., 28 August–5 September 1992.

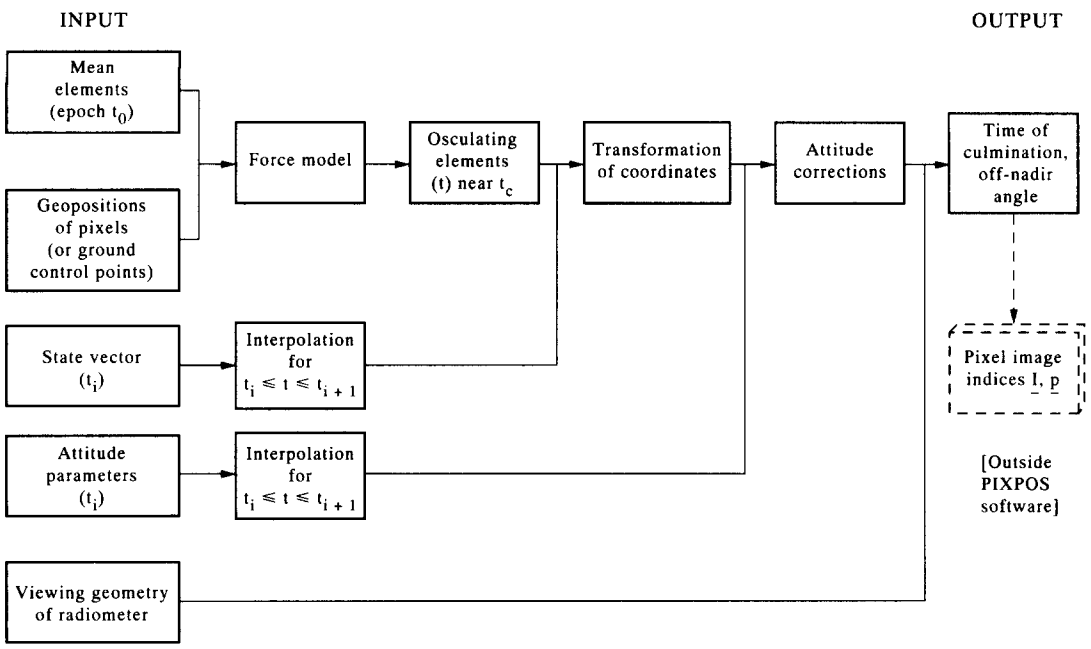

Fig. 1. Information flow during inverse referencing.

the gravity field of the Earth itself. We will represent this by the usual series of harmonic geopotential coefficients, appropriately truncated at a certain degree and order (Sections 2.3.1 and 2.3.2). Gravitational attraction of the Moon and Sun and indirect lunisolar perturbations due to the tides should also be mentioned. Of the various non-gravitational perturbations, the atmospheric drag (which leads to a secular decrease in the satellite's semi-major axis) and perturbations due to the solar radiation pressure should be investigated to decide if—for given orbit and satellite, and for given pixel size—it is necessary to account for these effects. A set of accelerations that cannot be neglected, constitutes the *force model* of the navigation software.

In principle, for low-accuracy orbital elements (such as "NASA 2-line", ORBITA-Intercosmos or the TBUS), the same force model that was used for the orbit computation should be used for the navigation. More detailed modelling of the orbit perturbations cannot be expected to lead to more accurate results for the inverse referencing when the orbital elements are poor (probably due to poor observations).

When orbital data of higher accuracy (or order 100 m along-track) become available, one should find a balance between loss of information from the original accurate orbit, due to an inadequate force model, and the use of too time-consuming navigation software with all small perturbations included; as an indication, we present Table 1.

Table 1 is based on Milani *et al.* [3] and Reigber [4] checked and amended by our own computations. Amplitudes of the accelerations due to various gravitational and non-gravitational sources for different satellites are presented to assess the force model necessary for a given purpose and for comparisons between various orbits. We work with this table more in Section 2.3.

The navigation software described below is partly a by-product of activity in ephemerides provision and orbit determination at the Astronomical Institute (AI) of the Czech Academy of Sciences [5,6]. As the need for improving existing software at the Hamburg

Table 1. Perturbing accelerations on orbits of artificial Earth satellites

Source of the acceleration	Magnitude of acceleration in ($m\,s^{-2}$) for the satellite				
	ERS-1	NOAA-N	STARLETTE	LAGEOS	GPS
Keplerian term	7.9	7.6–7.7	7.4	2.7	0.6
Earth polar flattening	9×10^{-3}	8.5×10^{-3}	8×10^{-3}	2×10^{-3}	5×10^{-5}
Geopotential (above $C_{2,0}$)	5.5×10^{-5}	5×10^{-5}	4.5×10^{-5}	6×10^{-6}	3×10^{-7}
Lunisolar perturbations	1×10^{-6}	1×10^{-6}	1×10^{-6}	2×10^{-6}	5×10^{-6}
Tides	2×10^{-7}	2×10^{-7}	2×10^{-7}	3×10^{-8}	1×10^{-9}
Maximum of atmospheric drag (secular trends!)	2×10^{-7}	2×10^{-9}	7×10^{-10}	3×10^{-12}	0
Solar radiation pressure	9×10^{-8}	5×10^{-8}	5×10^{-9}	4×10^{-9}	6×10^{-8}
Earth's albedo radiation pressure	3×10^{-8}	3×10^{-9}	1×10^{-9}	3×10^{-10}	1×10^{-9}
Relativistic correction	5×10^{-9}	5×10^{-9}	5×10^{-9}	1×10^{-9}	5×10^{-10}

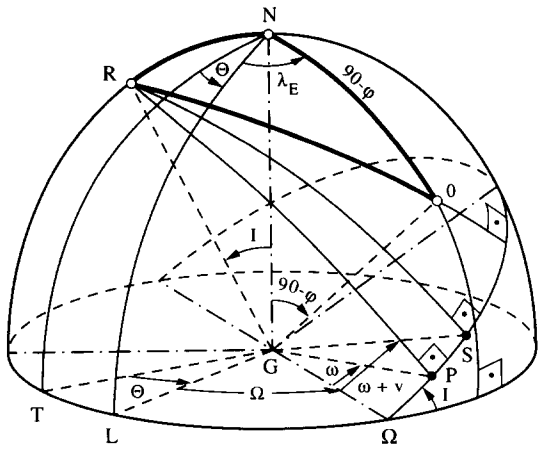

Fig. 2. Computation of time culmination: method of orbital meridian. Semi-major axis a, eccentricity e, inclination I, ascending node Ω, argument of perigee ω, mean daily motion n (in rev/day), mean anomaly M, true anomaly v, and (mean) sidereal time Θ, G, geocenter, R, orbital pole, N, North pole, O, observer, S, satellite, P, perigee, L, Greenwich meridian, T, vernal equinox. In this notation, angle LNO is the geocentric longitude and NGO the co-latitude of the station, $RGS = \pi/2$, $NGR = I$, $TNL = \Theta$, $TNR = \Omega - \pi/2$, $NRP = \omega - \pi/2$.

Institutes has been recognized, the original American software available for direct referencing, ORBITS, has been improved, and that for inverse referencing, PIXPO (where the inaccuracy was 10–15 pixels for the NOAA-N satellites mostly due to oversimplifications from the viewpoint of satellite dynamics), has been replaced by new programs PIXPO 3 and 4 [7].

The program EPHEM [5] as implemented for use on personal computers by Kostelecký [8] has been recognized as a useful tool for inverse referencing. EPHEM computes the ephemerides of artificial Earth satellites from given orbital data. It reports on a satellite's observability from one or more ground stations (with known coordinates) and yields detailed ephemeris data such as time, azimuth and elevation, for satellite tracking (Section 2.2.1). Let us replace the term "*satellite ground observing station*" by "*pixel*" and seek the instant when the pixel (station) and the satellite are on the same orbital meridian (Section 2.2.1, Fig. 2). It is the time of culmination of the satellite over the pixel. This is also the instant when the relevant line is scanned by the radiometer on board (at least for the NOAA-N satellites). The EPHEM program computes this time (among other quantities); thus, this program has been modified to PIXPO 3 (see Section 2.2.1).

In the program PIXPO 4, another method for computation of the culmination times (yielding potentially higher accuracy for inverse referencing) is used (Section 2.2.2). (Various subroutines for both programs PIXPO 3 and 4 come from the orbit determination and improvement program PRIOR [6] developed some time ago at Ondřejov Observatory.)

PIXPO 3 and 4 achieve the navigational accuracy roughly of the pixel size for the NOAA-N radiometers [7]. The main obstacle to an increase in accuracy is the low quality of the orbital elements available for the NOAA-N satellites.

Recently we added force models relevant to a pixel size of order 100 m (see Table 1) to both PIXPO 3 and 4 (the new programs are called PIXPO 3M and 4M). We also have prepared the program PIXPOSC, where the state vectors are used instead of the mean elements (Sections 3.5 and 5.2); the goal is to enable the navigation for ERS-1 with highly accurate "instantaneous coordinates" provided at close epochs (Section 3.5). Table 2 outlines the development of the software for inverse referencing.

The present state of the PIXPO's software package should fulfil the normal requirements posed by meteorologists. For extremely small pixel sizes (say 50 m), where even the improved force model used in PIXPO 4M would not be sufficient, the only program we may offer is PIXPOSC, based on the state vectors available.

The satellite images include several types of distortion that need to be corrected before the image data are used for remote-sensing applications. The errors can be subdivided into "orbital", "geometric" and "hardware errors". Table 3 summarizes them, giving rough values for their amplitudes, so their impact on the inverse referencing can be estimated.

2. METHOD

2.1. Our approach to inverse referencing

We use mean orbital elements (Sections 3.1–3.4) or rectangular coordinates with very small time separation (Section 3.5). Geodetic or geocentric

Table 2. Software package PIXPOS for the inverse referencing

Mean orbital elements			
Nadir pixel size of order–1 km	*PIXPO* Spherical approximation (1991)	*PIXPO 3* Standard (1991) based on EPHEM 5	*PIXPO 4* (1991–1992) new method for comp. time of culmination
Nadir pixel size of order 0.1 km		*PIXPO 3M* PIXPO 3 with improved force model (1992)	*PIXPO 4M* PIXPO 4 with improved force model (1992)
State vectors			*PIXPOSC* PIXPO for ERS-1 when $X, Y, Z, \dot{X}, \dot{Y}, \dot{Z}$ replace mean elements; culmination as in PIXPO 4, 4M; attitude corrections (1992–)

Table 3. Amplitudes of various distortions at inverse referencing

Error source	Type	Amplitude of error (m)
Inaccuracy of orbital elements or coordinates	Mean elements (NASA 2-lines, TBUS or similar)	1000–5000 along-track*
	state vectors (DGFI for ERS-1)	< 100 along-track
		~ 1 radially
Neglected gravitational perturbations (height 800 km)	Polar flattening (geodetic vs geocentric latitude)	20,000
	higher harmonics neglected	300 (often below 10 m)
	geoid undulations	110 (usually 10^1 m)
Neglected non-gravitational perturbations (height 800 km)	Atmospheric drag	See Table 5
Old values of basic constants		2000
Neglected scan skew efiect		700
Neglected timing error		560 m/day†
Neglected attitude parameters		1000†
Identification of pixel on map	Reading of coordinates of GCPs	500

*NASA [30].
†Emery *et al.* [2, p. 1176].

coordinates of a pixel (Section 1) are also given. If mean elements are available, the relevant force model (Section 2.3) is applied, and given mean elements from an epoch t_0 are transformed to osculating elements valid at time t as close as possible to the expected time of satellite culmination t_c over that pixel (or to the beginning of scanning for the particular scene). Then, we transform from the osculating elements to instantaneous satellite geocentric coordinates, i.e.

$$\mathbf{X}_S = f\,(\text{Keplerian elements}),$$

where f is the transformation for the Keplerian 2-body problem (see textbooks on celestial mechanics).

The satellite motion is usually described in an inertial (mean sidereal) coordinate system (terminology from Veis [9]), while the coordinates of GCP are related to the mean or instantaneous terrestrial system (rotating with the Earth). We rotate from/to terrestrial to/from inertial by means of the sidereal angle (time), accounting for nutation.

We seek the instant of satellite culmination over the pixel since at this instant the scanning takes place (see Sections 2.2.1 and 2.2.2). Finally we compute the zenith distance of the satellite as seen from the pixel at the culmination time. The off-nadir angle is computed from the given vector for the pixel $\mathbf{X}_D(x_D, y_D, z_D)$, and from the already computed satellite position vector $\mathbf{X}_S(x_S, y_S, z_S)$.

The Advanced Very High Resolution Radiometer (AVHRR) carried by the NOAA satellites of the TIROS-N series measures radiation with ground resolution between 1.1 and 6.1 km (at nadir, and at the largest scan angle of 55.38°, respectively). The scan direction is cross-track at a sampling rate of 1 line (2048 pixels) every 1/6 s. The time of each scan line is measured by uncalibrated satellite clocks. The timing for current NOAA-N satellites can be improved by introducing the calibration data from NOAA's Electronic Bulletin Board, to be accessed via the Omnet/Science Net.

The final step for inverse referencing, already outside our PIXPOS-software, is the computation of the pixel number p, from the off-nadir angle δ, and the pixel line l from the time of culmination t_c, via

$$p = (\delta_0 - \delta)\frac{2047}{2\delta_0} + 1 \tag{1}$$

where $\delta_0 = 55.38°$ is the maximum δ for the AVHRR, and

$$l = u(t_c - t_f) + 1, \tag{2}$$

where t_f is the time of the first line under consideration and u is the line rate (number of lines scanned/s).

The scanning geometry of the Along Track Scanning Radiometer (ATSR) on board ERS-1 differs from that for the NOAA-N satellites [10,11], so the software has to be modified accordingly (but this does not affect the computation of t_c). As all necessary details for ERS-1 are not yet at our disposal, the relevant changes will be made later.

2.2. Computation of time of culmination

2.2.1. Method of orbital meridian. The EPHEM program was conceived in the 1960s to support the project of laser observations of geodetic satellites and later on also to facilitate reception of telemetry data from the Intercosmos satellites. The main purpose was to select, as effectively as possible, time periods when the satellite is observable from a given location(s). To this end, a local culmination was defined as an instant when the satellite and the observing station are both on the same great circle passing through the orbital pole ("orbital meridian"). Such a geometrical situation could be found easily by an iteration process and then, at each culmination point, a simple test is used to reject not-observable positions (satellite would be below horizon or too low above it, in the Earth's shadow, during the day period at the station, etc.). A more detailed computation of parameters (azimuth and elevation of observable points, satellite slant range, data for automatic tracking by two-axes laser mount, etc.) is performed only for the observable passes.

Spherical trigonometry is used to transform the observer's position into the orbital coordinate system (Fig. 2). The basic spherical triangle NRO has two given (and for our purpose constant) sides NGO and NGR and an angle RNO which is an (almost linear) function of time according to

$$\mathrm{RNO} = \mathrm{TNL} + \mathrm{LNO} - \mathrm{TNR}. \tag{3}$$

Therefore

$$\cos \mathrm{RGO} = \cos \mathrm{NGO} \cdot \cos \mathrm{NGR} + \sin \mathrm{NGO} \cdot \sin \mathrm{NGR} \cdot \cos \mathrm{RNO} \tag{4}$$

$$\sin \mathrm{NRO} = -\sin \mathrm{ORN} = -\sin \mathrm{NGO} \cdot \sin \mathrm{RNO}/\sin \mathrm{RGO} \tag{5}$$

[and sign (cos NRO) = −1 if cos NRG · cos RGO > cos NGO]

$$\sin \mathrm{NOR} = \sin \mathrm{NGR} \cdot \sin \mathrm{RNO}/\sin \mathrm{RGO} \tag{6}$$

[and sign (cos NOR) = −1 if cos NGO · cos RGO > cos NGR].

The main idea is to use formulae (3)–(6) for transformation of the observer's position from a geographic coordinate system (defined by the equatorial plane and North pole N) to the orbital system (defined by the orbital plane and orbital pole R). The observer's "longitude" NRO in the new system can be determined from eqn (5) and the "longitude" NRS of the satellite from

$$\mathrm{NRS} = \mathrm{NRP} + v, \tag{7}$$

where classical formulae of celestial mechanics are used for computation of the true anomaly v from the mean anomaly M (which in turn includes perturbations caused by a stationary atmosphere) and terms up to quadratic are taken into account in the computation of the instantaneous position of ascending node [TNR in (3)] and perigee [NRP in (7)].

At the beginning of the time interval investigated, the angle

$$\mathrm{ORS} = \mathrm{NRS} - \mathrm{NRO} \tag{8}$$

has an arbitrary value, given by the orbital geometry at that time. At the instant of culmination, however, ORS = 0. If the first such instant is found (by the iteration method described below), each subsequent culmination is determined easily—it should occur one synodic period later.

The rate of change of the angle ORS is used in the iteration process to find the time of local culmination. A reasonable approximation of this rate ΔD for circular orbits is

$$\Delta D = n + \Delta\omega - (2\pi - \Delta\Omega) \cdot \sin \mathrm{NGO} \cdot \cos \mathrm{NOR}/\sin \mathrm{RGO}, \tag{9}$$

where the first two terms come from the satellite motion ($\Delta\omega$, $\Delta\Omega$ are daily changes of ω, Ω), and the third one from the projection of the observer's motion into orbital plane. The above formula holds only for low circular orbits, where the satellite moves substantially faster than the Earth rotates.

During the iteration process, two steps are involved. In the first one |ORS| should be less than 0.15 radians. If not, a time correction equal to ORS/ΔD is added and the computation repeated for this new "satellite-observer" configuration. If the first condition is satisfied, terms depending on eccentricity are added into formula (9) and a strengthened condition, $|\mathrm{ORS}| < \Delta D \cdot 0.00001$ radians, is applied. It was verified during several years of practical computations that, for satellites with moderate orbital eccentricity (up to 0.3), a "rough" correction is applied only at the beginning of the iterations and at most two small adjustments are necessary for determination of the subsequent culminations.

2.2.2. Method of perpendicularly crossing planes. Given is the position vector of the GCP $\mathbf{X}_D(x_D, y_D, z_D)$, usually in spherical coordinates geodetic latitude, longitude and height above "sea level" (φ, λ_E, h). Also we already know the position and velocity vectors of the satellite S at time t near t_c, i.e. $\mathbf{X}_S$, (x_S, y_S, z_S) and $\dot{\mathbf{X}}_S(\dot{x}_S, \dot{y}_S, \dot{z}_S)$. (They were computed from mean elements via osculating ones or they were interpolated from close state vectors.)

Now, let us assume two planes (Fig. 3):

(1) The plane $\rho\,(\mathbf{x}_T, \dot{\mathbf{X}}_S)$ is given by the unit vector $\mathbf{x}_T$, where $\mathbf{X}_T$ is the vector of local plumbline $\mathbf{X}_T(x_T, y_T, z_T)$, in S at t and by $\dot{\mathbf{X}}_S$ at t; $\mathbf{x}_T = \mathbf{X}_T/|\mathbf{X}_T|$. (The vectors $\mathbf{X}_T$ and $\mathbf{X}_S$ are not in general perpendicular!) We approximate the shape of the level surfaces at S and "at sea" by level ellipsoids, i.e. at the Earth's surface ("sea" for our purpose), by a best-fitting ellipsoid of revolution with semimajor axis a_{el} and flattening i_{el}. We neglect the difference due to a different shape of level surface at S and at sea (subsatellite point); our $\mathbf{x}_T$ is perpendicular to the level ellipsoid at the subsatellite point (this simplification is good enough for the present accuracy requirement and might be replaced by a more accurate model if necessary). For completeness we can write $\mathbf{X}_T(x_T, y_T, z_T) = f(\varphi_S, \lambda_S, h_S, a_{el}, i_{el}) = g(x_S, y_S, z_S)$, where $(\varphi, \lambda, h)_S$ are spherical coordinates of the satellite S(t) and $(x, y, z)_S$ its rectangular coordinates.

(2) Plane $\mu(\mathbf{x}_T, \mathbf{n})$ is given by $\mathbf{x}_T$ and the unit vector $\mathbf{n}$ perpendicular to the plane ρ, i.e. $\mathbf{N} = (\dot{\mathbf{X}}_S \times \mathbf{X}_T)$, $\mathbf{n}(n_x, n_y, n_z) = \mathbf{N}/|\mathbf{N}|$. Let us define also the vector $\mathbf{b}(b_1, b_2, b_3) = (\mathbf{n} \times \mathbf{x}_T)$, which is perpendicular to the plane μ, $\mathbf{b} = \mathbf{B}/|\mathbf{B}|$.

As the plane μ contains the point S, its equation can be written as

$$b_1 x + b_2 y + b_3 z - (b_1 x_S + b_2 y_S + b_3 z_S) = 0.$$

The scanning takes place when also the pixel D lies in the plane μ, and, therefore,

$$b_1(x_D - x_S) + b_2(y_D - y_S) + b_3(z_D - z_S) = 0 \tag{10}$$

which we solve iteratively by "shifting" the satellite along its orbit in small steps of time (or anomaly or by changing $\mathbf{X}_S$ and $\dot{\mathbf{X}}_S$).

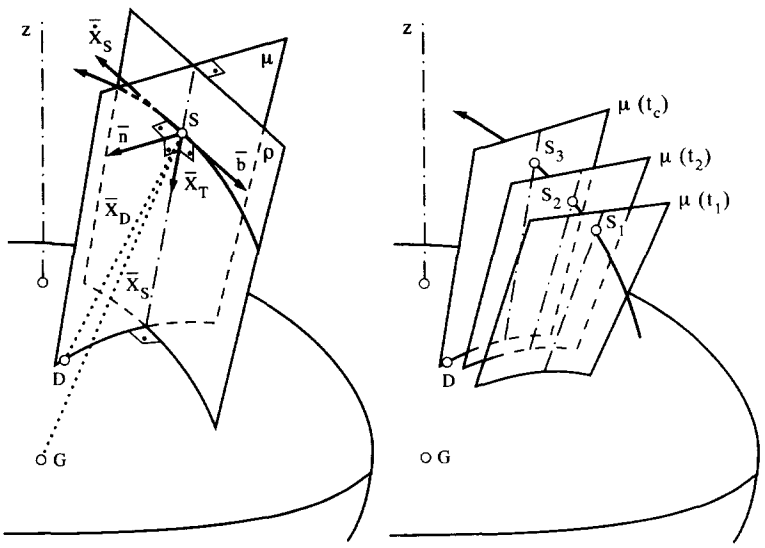

Fig. 3. Computation of time of culmination: method of perpendicularly crossing planes.

The culmination can be found in this way also:

$$\begin{bmatrix} n_x & n_y & n_z \\ x_D & y_D & z_D \\ x_S & y_S & z_S \end{bmatrix} = 0 \qquad (11)$$

by locating the instant when the determinant changes sign.

PIXPO4, 4M and PIXPOSC are based on (10); they do not use the orbital meridian (as in Section 2.2.1 and PIXPO 3, 3M). Thus, the PIXPO 4 (PIXPOSC) family is more general and potentially more accurate than the PIXPO 3 family (see also Section 4).

2.3. Force model

2.3.1. Sources of acceleration. The acceleration due to the Earth's gravitational field, lunisolar gravitation and various types of drag are given in Table 1 for ERS-1, NOAA-N, STARLETTE, LAGEOS and GPS (with average altitudes of 780, 800–850, 960, 5900 and 20,500 km, respectively). The non-gravitational accelerations depend on the area-to-mass ratio A/m of the particular satellite; the following values were used [m^2/kg]: 2×10^{-2}, 1.4×10^{-2}, 1×10^{-3}, 7×10^{-4} and 2×10^{-2}, respectively. Atmospheric drag leads to secular decrease in a and e, so we investigate its possible impact on inverse referencing (Section 2.3.4).

Table 1 answers which perturbations should be included for the required, prescribed accuracy (or pixel size) σ. The individual acceleration x_i has to be compared with that due to the spherical Earth (the "Keplerian term" in Table 1) x_0. We will include the particular source of acceleration in the force model if $(x_i/x_0) > \sigma/a$, where a is the semi-major axis of the satellite orbit.

Examples are given in Table 4.

For NOAA-N satellites and 1 km^2 nadir pixel size, a very simple force model with just $C_{2,0}$ would be sufficient (nearly compatible with the force model used for the "NASA 2-line" elements). For ERS-1, some low degree and order harmonic coefficients should be included (see Section 2.3.3); lunisolar perturbations are already small.

2.3.2. Gravitational perturbations. Long term perturbations due to the zonal harmonics as well as the short-periodic perturbations due to $C_{2,0}$ are computed according to Kozai's formulae [12, pp. 130–138]. Kaula's formulae [13, p. 40], are used for the tesseral harmonics. Lunisolar perturbations are computed from the formulae of Lundquist and Veis [12, p. 147]. The relevant subroutines are taken from the program PRIOR [6] or EPHEM [5]. Precision and nutation are computed by standard astronomical formulae [14].

To apply the Kaula formulae, the appropriate inclination and eccentricity functions are necessary. They have been studied intensively and—in addition to traditional formulae (Allan, Gooding, Kaula, etc.)—recent advanced software is available [15–18].

We have a database of Earth gravity field models at our disposal [19] from which we have—for PIXPO 3M, 4M—chosen the recent GEM T2 [20] and GRIM4S1 [21], truncated at degree and order 10 (Section 2.3.3).

The geoid undulations N can be added to the ellipsoid height h ($=0$ at sea, neglecting sea surface topography) in the input coordinates of GCP to improve navigation when a higher accuracy is needed. Extensive software, which computes geoid undulations (among other physical quantities) from

Table 4. Examples of force model

	For navigation		For geodynamics
	NOAA-N	ERS-1	LAGEOS
σ (m)	100	50	0.01
a (km)	7200	7153	12,250
Threshold	10^{-4}	10^{-5}	10^{-9}

an Earth gravity model, developed and kindly provided to us from the University of Karlsruhe [22] has been used.

2.3.3. Sensitivity analysis. The sensitivity of the particular satellite orbit to the individual harmonic coefficients C_{lm}, S_{lm} depends mainly on satellite semi-major axis and orbital inclination. Formulae for upper estimates of the total position effect, along-track, cross-track and in the radial direction are taken from Klokočník and Kostelecký [23] and used for ERS-1/NOAA-N orbits with recent gravity field models to $(l, m) = (50, 50)$. Our numerical results (program GRAVCIT) are reproduced in Straka *et al.* [24] and compare well with those from the program SENSI worked out in Deutsches Geodaetisches Forschungsinstitut (DGFI, Abt. 1, Munich); SENSI is based on a different definition of "orbital components" and is completely independent of our GRAVCIT. Our results agree also with Wakker *et al.* [25]. A graphical representation of the sensitivity (computed by SENSI) for ERS-1 is, for example, in Reigber [4] or Reigber *et al.* [26].

For ERS-1 (50 m threshold for a 500 m^2 pixel size), we should include odd zonal harmonics to about degree 30 and tesseral harmonics roughly to $(l, m) = (4, 4)$. In a detail, the sensitivity for the first order and resonant orders is higher (namely along-track), so we should include the terms up to degree about 8 for the first order, the first few harmonics of the 14th and 15th orders (shallow resonances) and the first few harmonics of the 43rd order (deep resonance).

The question is whether the analytical solution of satellite motion underlying the PIXPOS software [13,27,28] still works well for a deep resonant regime; it seems to be so [29]. As the phenomenon of resonance is interesting not only for navigation, its further investigation is under way (Lagrange planetary equations, for the resonant indices, will be integrated numerically, and the results will be compared with those based on the original analytical formulae).

2.3.4. Non-gravitational perturbations. Table 1 indicates that the atmospheric effects might be of interest. A simple atmospheric density model would be sufficient to test the effect and to compare the model with the very simple empirical approximation to drag, as prescribed with the "NASA 2-line" elements in NASA [30], (Section 3.1) and with the "implicit" drag in the TBUS elements (see Section 3.2). As, in the Ondřejov Observatory, the TD 88 thermosphere model has recently been developed [31] and we implemented [32] the relevant software in PIXPO 3, for test purposes.

TD 88 describes the distribution and variation of the total atmospheric density over a specific surface at a constant height over the oblate Earth, with the help of a series of spherical harmonic coefficients (analogous to the geopotential coefficients). The model is valid within the height range of 200–800 km, for a solar 10.7 cm flux index from 60 to 220 and the geomagnetic activity index 0–9. The effect of the atmospheric drag on the orbital elements has been developed from the equations of motion, the underlying theory being in Sehnal [32].

Numerical results are presented in Table 5. They can be mapped into "along-track" error of time of culmination ΔT, by means of third Kepler's law ($\Delta T = -1.5\,\Delta a T/a$), where Δa is the change of a (from Table 5) and T is orbital period ($n = 2\pi/T$). Our interpretation is the following:

(1) For a pixel size of 1 km^2, NOAA-N orbits and reasonably "fresh" orbital elements (not older than about 2 weeks), we can model the effect of atmosphere according to NASA [30] or NOAA/NESS [33]. We do this in PIXPOS software. Note that the TBUS elements (Section 3.2) are available every day, so the effect of the atmosphere from the epoch to the time of a scene could be neglected.

(2) For a pixel size of order 100 m and the lower orbit of ERS-1 type, we would need an atmospheric density model. Fortunately, "instantaneous" state vectors may be used instead of mean elements for ERS-1, and thus, we need no perturbation model.

The other accelerations of non-gravitational origin are (Table 1) comparable or lower (for ERS-1 and NOAA-N satellites) than that due to the atmosphere and give rise to periodic changes in the orbital elements. Hence, we neglect them.

Table 5. Effect of the atmosphere on the decrease of the semi-major axis for NOAA-N and ERS-1 satellites

Satellite	a (km)	e	I (deg)	10^2 A/m (m^2 kg^{-1})	Solar flux min/max	Geomag. index k_p min/max	Decrease Δa (m/x-days) x = 5 days	x = 15 days	x = 30 days
NOAA-N	7230	0.002	99.06	1.4	60	0	2	6	14
						9	3	10	20
Odd					220	0	25	78	169
numbers						9	37	117	254
NOAA-N	7190	0.002	98.65	1.4	60	0	3	10	20
						9	5	16	31
Even					220	0	37	109	216
numbers						9	55	164	324
ERS-1	7150	0.001	98.52	2.0	60	0	7	18	37
						9	9	28	56
					220	0	47	141	289
						9	71	211	434

3. ORBITAL DATA

3.1. "NASA 2-line" mean orbital elements

The U.S. "two line orbital elements, NASA GSFC" actually originate from the USAF and are based on observations of limited accuracy, since it is an USAF aim to track all objects in low orbits. These elements were used for a long time in the EPHEM program, where they were labelled "NASA 2-line" elements. They have been described in NASA [30]. A highly truncated Earth gravity model is used for orbit computation ($C_{2,0}$ and $C_{3,0}$ only, the first order analytical theory for the motion of a satellite due to Kozai [28] being cited in NASA [30]). The mean motion n is given instead of a; for their relationship as defined by Kozai, also given in Attachment B of NASA [30], see Section 3.3. The time derivatives of n are included in the 2-line elements; they are used to model the secular decrease in a and e due to (total) drag.

These elements sometimes suffer from long time gaps (more than 14 days) between successive sets. If they are sufficiently recent, they permit position computation to an accuracy of ± 1 to ± 5 km [30; NOAA, private communication].

3.2. TBUS mean elements

The TBUS elements are available from NOAA/NESS [33]. These are "Brouwer mean elements". The Brouwer [27] and Brouwer–Lyddane analytical theory is an alternative theory to Kozai's describing satellite motion in the Earth's gravity field [34] with only the zonal harmonics to $C_{5,0}$.

The original information for the NOAA/TBUS elements comes from the USAF (NORAD) so-called "4-line" elements, a Cartesian vector and a ballistic coefficient to keep track of the drag. The elements were computed from a 10 day observation file for the last days observations (but no details about the proper procedure for orbit computation from observations are at our disposal). The observations are radio-interferometric directions (minute of arc accuracy). The force model is a modified Brouwer theory with some tesseral harmonics and acceleration of the mean anomaly to cover the drag.

NOAA (private communication) takes the NORAD vector and ballistic coefficient and generates updated Cartesian vectors (through the NASA Goddard Trajectory Determination System), numerically integrated with a full gravity field model (!), and the Brouwer mean elements [33]. NOAA merely converts the state vectors minute by minute according to Brouwer–Lyddane theory.

We treat the NASA 2-line and the TBUS elements as mutually independent data, but the observations used to generate the elements might overlap. The low accuracy of observations can easily explain a kilometer difference between results of inverse referencing with these two types of elements (see Section 5.1).

The advantage of the TBUS elements over the "NASA 2-line" elements is their daily issue so they are always fresh. In the Hamburg Institutes, they are accessible for current radiometer scenes from the NOAA's Electronic Bulletin Board.

The TBUS elements provide a, not n, in contrast to the NASA 2-line elements. For the relationship between them see Section 3.3.

3.3. Remarks on the mean elements n and a of Kozai and Brouwer

The precise meaning of the orbital elements published by a particular organization has often been a source of difficulty to users, since a degree of arbitrariness is inherent in any definition. The problem centres on the removal of short-period perturbations due to J_2 ($= -C_{2,0}$) from osculating elements, to permit the dissemination (at particular epochs) of steadily varying "*mean*" elements, and the arbitrariness arises because the "zero" of "*sh-p pert*" (short-periodic perturbations) in the split symbolized by "*el(osc) = el(mean) + sh-p pert*" is not uniquely defined. In the present use of two-line and TBUS elements we are only concerned with the (related) elements a (semimajor axis) and n (mean motion), but a full account of the problem has been given elsewhere [35–37], for all the elements and for zonal harmonics not limited to J_2.

The most widely used sets of orbital elements have been those based on the theories of Kozai [28] and Brouwer [27]. The two-line elements are Kozai-based and TBUS elements Brouwer-based, so we attach suffices K and B to the respective values of the mean elements n and a. The following point is important: though the osculating n and a necessarily satisfy Kepler's third law, $n^2a^3 = GM$, precisely, this does not have to be so for mean n and a, if there is a compelling reason for separate definition. In practice, the relation does hold for n_B and a_B, but n_K and a_K satisfy an off-set relation [GM is the geocentric gravitational constant].

In the two-line adoption of Kozai's theory, it is n_K that is provided, a_K being a quantity derived from the relation

$$n_K^2 a_K^3 = GM\{1 - \tfrac{3}{4}J_2(R/a)^2(2 - 3\sin^2 I)(1 - e^2)^{-3/2}\} \tag{12}$$

which involves the mean elements e and I as well as n and $a(= a_K)$. The definition of n_K is felicitous in that the following two properties both hold: n_K is the same as the quantity n' [35–37] that arises naturally from the exact energy constant for a J_2-alone (conservative) field; also n_K is the rate of change of the "mean mean anomaly", M_K. (This identity of role does not extend to the other zonal harmonics, or beyond the first order in J_2.) The definition of a_K (by the above formula) is not so felicitous and the use of a', such that n' and a' satisfy Kepler's law without offset, might have been preferable but this is of no relevance

here, because a_κ is supplied by the two-line orbit generator.

In the TBUS adoption of Brouwer's theory, a_B is provided and n_B is derived from the Kepler law without any offset. This is not the same as n_κ, however, so to derive "two-line-equivalent elements", we apply the formula

$$n_\kappa = n_B\{1 + \tfrac{3}{4}J_2(R/a)^2(2 - 3\sin^2 I)(1 - e^2)^{-3/2}\}, \tag{13}$$

which may be identified (to first order in J_2) with the formula given in a footnote of Brouwer [27] wherein our n_B is denoted by n_0 and the time integral of n_κ (i.e. M_κ) by l''. To complete the transition to two-line-equivalent elements, it then only remains to replace a_B by a_κ, using the formula (12) that derives a_κ from n_κ.

3.4. Other types of mean elements

EPHEM 5, PIXPO 3M, 4, 4M are able to read and work with the following types of orbital data: injection point parameters; so called "NASA 2-line" elements (Section 3.1); ORBITA code (Russian elements from Institute for Space Research, Moscow); U.S. five-line elements; SAO-CNES telex code; ZIPSAT code; Farnborough elements [38]; orbit from position and velocity; and the TBUS elements (Section 3.2). The various types are "unified" within the subroutine INEL.

3.5. State vectors

These comprise geocentric position and velocity coordinates X, Y, Z, $\dot{X}$, $\dot{Y}$, $\dot{Z}$ at close epochs t_i. For ERS-1, they are computed by the Deutsche Geodaetische Forschungsinstitut/German Processing and Archiving Facilities (DGFI/D-PAF) in Munich and Oberpfaffenhofen, and accessible via the ERS-1 Central user Service at Earthnet ERS-1 Central Facility at ESRIN, Frascati, Italy.

The preliminary/precise (definitive) orbits consist of the state vectors in CIS (Conventional Inertial System, non-rotating with the Earth) and in CTS (Conventional Terrestrial System, rotating with the Earth), and of time (in TDT, Terrestrial Dynamic Time). Also the attitude parameters of ERS-1 (*roll*, *pitch* and *yaw* angles in 0.001 deg) are added, as well as some orbit-quality parameters. All these data are available every 120 or 30 s for the preliminary/precise orbits, respectively.

The orbit determination of ERS-1 by DGFI is based mostly on laser observations (PRARE on board ERS-1 does not work); the expected accuracy is of the order of tens of meters along track and about 1 m radially (with a GRIM 4 version of gravity model and the best orbit determination software, Schwintzer *et al.* [27]; Massmann, private communication).

In the program PIXPOSC, we interpolate for t to be as close as possible to t_c, using state vectors at the adjoining epochs. A special subroutine for the interpolation procedure (kindly provided with American altimeter data from GEOSTAT) is one of the options in the program.

4. ATTITUDE CORRECTIONS FOR INVERSE REFERENCING

The attitude parameters yaw Y, pitch P, and roll R can be defined as follows [39]: the yaw axis is directed toward the nadir on the local vertical, defined by X_T, the pitch axis is directed towards the negative orbit normal, and the roll axis is perpendicular to the other two such that unit vectors along the three axes have the relation $\mathbf{R} = \mathbf{P} \times \mathbf{Y}$. Thus, in a circular orbit, the roll axis will be along the velocity vector. The roll, pitch, and yaw angles (a_{roll}, a_{pitch}, a_{yaw}) are defined as right-handed rotations about their respective axes.

The attitude parameters are an integral part of the state vectors of ERS-1, computed by DGFI/D-PAF. They are given with the same time resolution (30 or 120 s for the precise or preliminary orbits) as the coordinates and velocity components; their accuracy is about 0.11 deg (pitch, roll) and 0.21 deg (yaw), according to Vass and Handoll [11].

For inverse referencing, we need to know the relation between the inner satellite coordinate system (defined by the reper $\mathbf{x}_B$ of the unit vectors (R', P', Y') and the inertial or terrestrial geocentric system (in which the satellite's motion is described). The pitch roll and yaw, (RPY)-system, can be used for this purpose. Then

$$\begin{aligned} x_B &= |R', P', Y'|^{\mathrm{T}} \\ &= A \cdot |R, P, Y|^{\mathrm{T}} \end{aligned}$$

where

$$A = \begin{bmatrix} 1 & a_{\text{yaw}} & -a_{\text{pitch}} \\ -a_{\text{yaw}} & 1 & a_{\text{roll}} \\ a_{\text{pitch}} & -a_{\text{roll}} & 1 \end{bmatrix}. \tag{14}$$

The next step is to relate (RPY)-system to the geocentric one,

$$\begin{aligned} P &= (X_S \times \dot{X}_S)/(|X_S \times \dot{X}_S|), \\ Y &= -X_T/|X_T|, \\ R &= P \times Y. \end{aligned} \tag{15}$$

There is a sign difference for the yaw axis, which results also in a sign difference for the roll axis in the data provided by the DGFI/D-PAF, namely $a_{\text{yaw(DGFI)}} = -a_{\text{yaw}}$, $a_{\text{pitch(DGFI)}} = a_{\text{pitch}}$ and $a_{\text{roll(DGFI)}} = -a_{\text{roll}}$.

5. NUMERICAL RESULTS OF INVERSE REFERENCING

5.1. Results and validation tests for NOAA-N satellites

One example of the input/output of our PIXPO's software (program PIXPO 4M for TBUS elements of NOAA-9) is given in Table 6(a,b). The points "6001" to "6006" are real Ground Control Points (GCPs) of the scene "6" of the radiometer on NOAA-9. Given

Table 6(a, b). Input/output of PIXPOS software

Input sample:

```
9    5     0.0833
87.  1.  8.  20.  7.  24.470  0.00154  295.150  333.320  99.029  7229.672  170.142
870110  14  09  00  0.00  0.0  00000
6000     0.0        13.18  0.0
6001     54.7417    8.2917  0.0
6002     55.0583    8.4333  0.0
6003     55.5833    8.0833  0.0
6004     56.7000    8.2167  0.0
6005     58.1083    6.5667  0.0
6006     59.3083    4.8667  0.0
```

Description of the input sample:
First line:
(a) (b) (c)

- (a) type of elements, 2 for NASA-2 line, 9 for TBUS elements; for more details see subroutine INEL in all versions of PIXPO 3 and PIXPO 4 programs;
- (b) max. degree of zonal harmonics (max. 5 is permitted); standard use: 3 for NASA 2-line and 5 for TBUS elements;
- (c) scan skew effect (s).

Second line:
TBUS elements:
(1) epoch:
Y M D H MIN S ..... the epoch of the mean elements (UTC),
(2) the elements themselves (free format just for the TBUS elements):
eccentricity, argument of perigee (deg), longitude of the ascending node (deg), inclination (deg), semi-major axis (km), mean anomaly in epoch (deg).
For more details see NOAA/NESS [33].

USAF elements called here "NASA 2-line elements":
for detailed description see NASA [30] or (Klokočník *et al.* [7].

Third line:
Y M D H MIN S "initial" time of scene, time of the first line in the consideration, or time just before the nearest equatorial crossing.
UT1–UTC time correction between "rotational" UT1 and "world coordinated" UTC time scales (BIH Annual reports) (s),
rate (UT1–UTC) rate of this correction (s/day),
epoch (UT1–UTC) (integer) modified Julian date for which the correction applies (BIH Annual reports).
standard use: put zeros for the last 3 quantities.

Next n-lines for n-points (these points may be Ground Control Points):

Input coordinates (free format, recommended number of valid digits approx. as in our example):

Point No.
its GEODETIC latitude (not geocentric) (deg),
longitude (East of Greenwich) plus–minus 0–180 (deg),
height above sea level (or geoid undulation) (m).

Output sample:

```
SATELLITE:        NOAA-9
  SOURCE OF ELEMENTS:     TBUS
  EPOCH:                  46803  0.838478  8.  1.1987  20:  7:24.47
  PERIG:    295.150000   -2.811648     (deg)     (deg/day)
  RNODE:    333.320000    1.005658
  INCLN:     99.029000
  ECCEN:      0.001540
  SAXIS:   7233.902                    (km)
  MANOM:      0.472617   14.114687     (rev)     (rev/day)
```

Identification of the program:

PROGRAM PIXPO4M

Step of computation of culmination times (standard use: 10–60 s).

STEP IN COMPUTATION [s]: 10.00

Options for the force model:

GRAVITY FIELD PERTURB. TO DEGREE AND ORDER 6 INCLUDED, NOW GEM-T2
LUNI-SOLAR PERTURB. ARE INCLUDED
LONGPERIODIC ZONAL TERMS (J3 AND J5) INCLUDED:

Standard use for NOAA-N satellites:

Standard use for NASA 2-line elements: "gravity field perturb. 0"
"lunisolar 0, not included"
"zonals 3",
"resonances 0, not included".

Standard use for TBUS: "gravity field perturb. 2–6"
"lunisolar 0, not included"
"zonals 5", see the data file.
"resonances 0, not included".

Main results:

	INPUT			OUTPUT		
Point No.	geodetic latitude (deg)	E. longit. (deg)	height (m)	time of culmination D M Y H MIN S		off-nadir angle (deg)
6001	54.741700	8.291700	0.0	10. 1.87	14:24:52.842	−39.3524
6002	55.058300	8.433300	0.0	10. 1.87	14:24:58.062	−39.8172
6003	55.583300	8.083300	0.0	10. 1.87	14:25: 7.348	−39.3608
6004	56.700000	8.216700	0.0	10. 1.87	14:25:26.224	−40.2028
6005	58.108300	6.566700	0.0	10. 1.87	14:25:51.845	−37.6352
6006	59.308300	4.866700	0.0	10. 1.87	14:26:14.135	−34.7987

are the orbital elements and the geodetic coordinates of the GCPs; the results are the time of culmination t_c and the off-nadir angle δ. We have chosen various salient features in the coastlines of the North Sea acting as the GCPs [7]. Their geodetic (geographic) coordinates were resolved from Internationale Kartenserie Nordsee (European Datum, WGS 84), with uncertainties between 0.2 and 0.5 km. As the AVHRR (NOAA-N) pixel size is between 1.1 and 6.1 km and the accuracy of the elements themselves permits 1–5 km navigational accuracy (Sections 3.1 and 3.2) if the elements are recent enough, the error in the coordinates of GCPs due to the reading from the maps is still acceptable.

The validation of inverse referencing techniques can be performed in different ways:

(i) Intercomparison of location of a satellite, of the culmination time and the off-nadir angle as derived from different and independent navigation software, see tests with PIXPO 3 and PIXPO 4, 4M, partly independent, with PIXPO 3/4M and PIXPOSC (mutually independent), and by means of "direct" vs "inverse" referencing with the programs ORBITS (ORBITEST) and PIXPOS.

(ii) Intercomparison of t_c and δ as derived from sets of orbital elements of different age (this method may be called "artificial aging" of the elements).

(iii) Comparison of inversely referenced images with known locations (geodetic coordinates) for salient features that can be detected in the images ("method of actual GCPs").

(iv) Intercomparison of inversely referenced images of the same scene from different imaging satellites or from different passages of the same satellite ["overlapping scenes", Fig. 4(a, b)].

Table 7 shows t_c and δ for the two GCPs arbitrary chosen from several scenes from NOAA-9. We can compare the results from our PIXPOS software with the AVHRR observations [7]. Further, we can study the differences Δt_c and $\Delta\delta$ due to the type of orbital elements used, see line ⟨2⟩ vs ⟨1⟩, ⟨4⟩ vs ⟨3⟩ of Table 7, due to the method of computation of t_c, ⟨3⟩ vs ⟨1⟩, ⟨4⟩ vs ⟨2⟩, and due to the force model accounted for in different details, ⟨4⟩–⟨9⟩. Added are estimates for the effect of atmosphere (Section 2.3.4), namely ⟨10⟩ vs ⟨1⟩ of Table 7, of the neglected geoid undulation, ⟨11⟩ vs ⟨9⟩, and due to an inclusion of short-periodic perturbations according to Brouwer theory ⟨12⟩.

The difference due to the use of TBUS or NASA 2-line elements (mutually as close epochs as possible were selected) sometimes achieved $\Delta t_c \sim 0.4$ s (~ 3 km along track); the difference $\Delta\delta$ was smaller. This result coincides well with the accuracy of the elements described above.

The difference due to the method of computation of t_c becomes important also, $\Delta t_c < 0.4$ s. We have numerically verified that this type of Δt_c equals zero for $\phi = 0$ and $\pm\phi = I$ (which is expected from

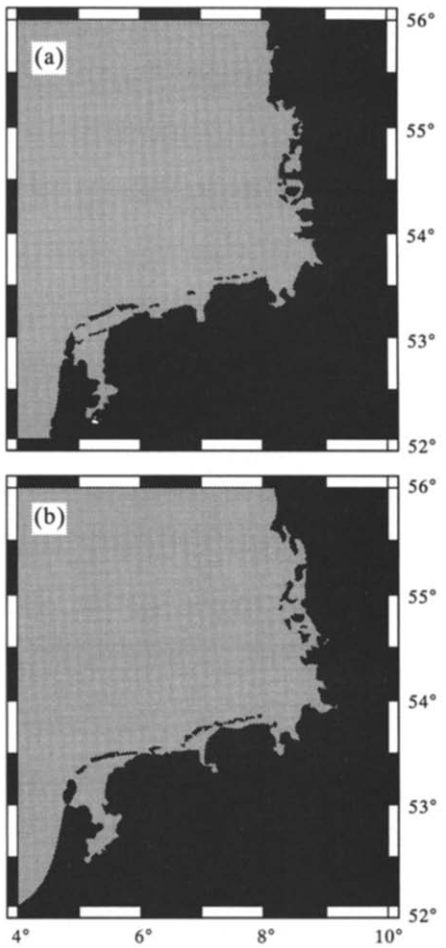

Fig. 4. Inversely referenced AVHRR images obtained from NOAA-9 on 10 and 11 August 1987. The images are superimposed on each other, black indicates land surfaces, water surfaces are grey shaded, (a) referenced with PIXPO, and (b) referenced with PIXPO 3.

comparison of Fig. 2 with Fig. 3). PIXPO 4 program family is potentially more accurate than PIXPO 3 family.

The more detailed "force model" means that we include step by step the effects of J_5 to the simplest "force model", where just the effects due to J_3 were accounted, then C_{22}, S_{22} are added to J_3, J_5, etc. to C_{99}, S_{99}, see Table 7. For the NASA 2-line elements, J_5 is already "illegitimate" since J_5 is not included in the perturbation model of these elements [8]. Inverse referencing with the TBUS elements should keep J_5, however; we found $\Delta t_c \sim 0.15$ s ($\sim$ nadir pixel size) due to J_5. In our examples, the tesseral harmonics C_{22}, S_{22}, for the TBUS elements still "legal", lead to $\Delta t_c \sim 0.05$ s in comparison with the previous "zonal case". The terms above degree and order 6 can be neglected as well as the luni-solar effects. The results compare well with the estimates in Table 1.

The computer time required increased from PIXPO 3 to PIXPO 4. For example, the scene shown by Tables 6(a) and (b) needed 0.2 s of user time on our

Table 7. Examples of results of inverse referencing for comparison

NOAA-9 scenes		Point No. 3007 19 August 1987		Point No. 6001 10 January 1987	
⟨ ⟩	Program, elements force model	t_c (s) 14 h 57 min	$-\delta$ (deg)	t_c (s) 14 h 24 min	$-\delta$ (deg)
—	AVHRR	49.88	28.50	52.35	39.32
⟨1⟩	PIXPO 3 NASA J_3	49.60	28.54	52.21	39.35
⟨2⟩	PIXPO 3 TBUS J_3	49.37	28.53	52.27	39.33
⟨3⟩	PIXPO 4 NASA J_3	49.92	28.54	52.58	39.35
⟨4⟩	PIXPO 4M TBUS J_3	49.66	28.53	52.65	39.34
⟨5⟩	PIXPO 4M TBUS J_2, J_5	49.819	28.538	52.758	39.345
⟨6⟩	PIXPO 4M as ⟨5⟩, plus C_{22}, S_{22}	49.875	28.551	52.821	39.350
⟨7⟩	PIXPO 4M as ⟨6⟩, to C_{66}, S_{66}	49.897	28.553	52.842	39.352
⟨8⟩	PIXPO 4M as ⟨6⟩, to C_{99}, S_{99}	49.902	28.552	52.849	39.351
⟨9⟩	PIXPO 4M as ⟨7⟩, plus luni-solar	49.885	28.551	52.821	39.352
⟨10⟩	PIXPO 3 as ⟨1⟩, plus atmosphere TD88	49.638	28.540	52.213	39.351
⟨11⟩	PIXPO 4M as ⟨9⟩, plus geod undul., 100 m	49.885	28.554	52.821	39.349
⟨12⟩	PIXPORB 5 comparable to ⟨5⟩	49.234	28.581	52.589	39.388

SUN SPARC station for the 6 points with PIXPO 3 (J_3, J_5), 0.4 ⟨0.5⟩ s with PIXPO 4M (J_3, J_5), and 0.4 ⟨26.5⟩ s with PIXPO 4M (J_3, J_5, tess. to 6,6 plus luni-solar, see Table 6(b). The times in the angle brackets are needed to compute the perturbations (but this is done only once per scene). A further reduction is by selecting the time of the first line as close as possible before its t_c.

To avoid an objection that our software yields reasonable results just for a certain geolocation and for the orbits of NOAA-N satellites (all similar), we tested PIXPO 3 and 4M by means of "artificial scenes", where no real GCPs exist. First, we used the American program ORBITS (its improved version ORBITEST [7]) for direct referencing, i.e. we computed subsatellite points. The times of culmination over them were then sought inversely by the PIXPOS software. ORBITEST and PIXPOS are independent, both can work with the TBUS elements. The tests were run for NOAA-9, 12 and AJISAI satellite ($I = 50$ deg, $a = 7800$ km) for various places over the globe. The difference Δt_c between ORBITEST and PIXPOS ranged between 0.0 and 0.7 s, $\Delta\delta < 0.3$ deg. The more detailed force model helped to decrease Δt_c, but not always. The differences Δt_c have a complicated geographical signature. In general, no systematic errors which might be attributed to a certain geolocation or orbit have been found.

Sometimes the orbital elements available were too old and inverse referencing with PIXPO 3 or 4, 4M failed. To investigate the effect of "aging" of the elements, we computed the same scenes repeatedly with elements of various ages. We used several scenes and both types of elements. The scenes computed with the TBUS elements inclined to rapid and very irregular degradation with time (sometimes even after 1 week Δt_c was above 1 s, ~8 km along track). It seems the procedure DELTAE, accounting for the drag of the NASA 2-line elements (Section 3.1), helps to cover the drag even for 14-day-old elements; for the TBUS elements, no similar procedure is available. It is evident that the user should use the freshest elements possible. If the results are not satisfactory, the adjoining elements (next or previous epoch) should be used (to avoid a gross error in transmission of elements of the particular epoch). In the Hamburg Institutes, the TBUS elements for recent scenes are now available every day (Section 3.2), so the problem of "old elements" is eliminated.

The time t_c is solved iteratively in the PIXPO 4 and PIXPOSC family [eqn (10), Section 2.2.2]. The time step Δt of this iteration should not be too large (to avoid a loss of accuracy of t_c) or too short (excessive computer time). Our previous tests indicated the optimum $\Delta t \sim 10$ s [7] and now we see that $\Delta t \sim 10$ to 30 s is quite adequate. For $\Delta t = 300$ s, an offset of t_c with respect to t_c computed with $\Delta t = 10$ s was 0.02 s.

The programs ORBITEST and PIXPO 4M were also used for a test of their "internal consistency". The satellite's rectangular geocentric coordinates were generated by these two programs independently for exactly the same instant, and compared. The

Table 8

Point No.	Geodet. lat. φ	Longitude (E) λ	PIXPOSC state vectors t_c (h:m:s)	PIXPOSC state vectors $-\delta$ (deg)	PIXPO 3 NASA 2-line t_c (s)	PIXPO 3 NASA 2-line $-\delta$ (deg)	PIXPO 4M NASA 2-line t_c (s)	PIXPO 4M NASA 2-line $-\delta$ (deg)	Age of elements (days)
2222	73.8673	194.3568	15:36:41.87	62.00	41.68	62.58	41.65	62.58	0.05
					41.01 (37:)	62.60	40.98	62.60	−9.5
3800	81.3600	2.9387	15:38:00.00	0.05	59.95	0.06	59.95	0.06	0.05
					59.34	0.06	59.33	0.06	−9.5
5030	−9.1379	86.2063	16:50:30.00	0.00	29.33	0.09	29.26	0.10	0.05
					29.88	0.07	29.82	0.08	−9.5
5000	0.0000	84.0000	16:53:04.173	1.43	03.79	1.38	03.79	1.38	0.05

position difference is around 10 m, which indicates that all transformations in both programs are correct.

While the first two methods (i) and (ii) mentioned above are independent of any imaging radiometers, the last two techniques require an imaging instrument that resolves salient ground features with an accuracy that is to be validated as the accuracy of the inverse referencing. This means that if we want to verify a 1 km accuracy for inverse referencing, we have to identify objects within the image with a resolution of at least 1 km. In the case of the NOAA spacecraft we can use the AVHRR that scans in cross-track mode resolving 1.1 km at nadir view and 6.1 km at the greatest scan angle of 55.38°. Hence, restricting ourselves to the near nadir fields of view we are able to validate the referenced images with accuracies of about 1 km.

We have chosen fifteen different GCPs along the coast lines of the North Sea and identified them in six different AVHRR images as retrieved from the NOAA-9 orbiter. The mean differences as obtained with PIXPO 3 range from 0.26 to 1.33 km when using orbital elements with an age of 1.9–6.4 days, respectively [7]. The results as obtained with the simple circular orbit model, PIXPO, starting from a known equator crossing, are far worse and not useful for an image geolocation. This is demonstrated by images as retrieved from NOAA-9 passages over the North Sea on 10 and 11 August 1987. The data have been geolocated by the methods under consideration and gridded to a mercator projection in the area bound by the coordinates 52°N, 4°E and 56°N, 10°E. Land surfaces are black, and water grey shaded. The images for the two days are superimposed. Figure 4(a) clearly shows that the simple method produces errors of more than 20 km when compared with the advanced technique [Fig. 4(b)]. Even the superimposed images from the successive days do not match each other, as is seen by the duplicated islands near 53.5°N, 5.5°E. The result of the advanced technique, seen in Fig. 4(b), shows an agreement of successive images within narrow limits uniquely reproducing the real coastlines.

5.2. Tests for ERS-1

We have two samples of the state vectors of ERS-1 (Sections 3.5 and 4), one overlapping with the NASA 2-line elements. The comparison "PIXPOSC vs PIXPO 3 or 4M" with NASA 2-line mean elements can put some light on the accuracy of these elements, because the state vectors of ERS-1 can be considered as practically errorless in this test. Moreover, these two types of programs are mutually independent, so an agreement of their results yields a very useful software check. The comparison has been performed for the GCPs in the North Sea as well as for the artificial scenes around the globe; the age of the NASA 2-line elements was between 1 and 10 days with respect to the epoch of the state vectors. The typical results are given in Table 8.

A typical Δt_c between PIXPOSC and PIXPO 3 or 4M is a few tens of seconds, compatible with the accuracy of the NASA 2-line elements (if they are fresh) and in good agreement with the results from Section 5.1.

We have also compared the rectangular geocentric coordinates of the satellite computed for arbitrary instants by PIXPO 4M with those interpolated from the state vectors; the difference is from hundreds of meters to tens of kilometers (for the NASA elements for the Z-axis).

The attitude parameters enter via matrix A (14); in our samples, the pitch angle varies between $+0.05$ deg and -0.05 deg, the roll between ± 0.2 deg, and the yaw angle is in the range of ± 3.9 deg. These values are still "small", as required by eqn (14). They are published to 2–4 digits, but only 2 digits are usually significant (see Section 4). The rate of change of the attitude parameters is "smooth" enough, so a linear interpolation between the state vectors for these parameters should be sufficient. For the coordinates and velocities, however, we make use of interpolation by Hermite polynomials (Section 3.5).

6. CONCLUSION

Navigation (namely inverse referencing) for meteorological satellites NOAA-N and the remote sensing satellite ERS-1 has been studied and the software package PIXPOS has been developed and applied to radiometer observations from NOAA-N satellites.

The programs PIXPO 3 (in routine use at the Hamburg Institutes), PIXPO 4, PIXPO 4M, and PIXPOSC are available, in FORTRAN 77 on one floppy disk, for scientific exchange.

Extensive validation tests confirm that the software enables inverse referencing with an accuracy relevant to the TBUS or NASA 2-line mean orbital elements which is compatible to the nadir pixel size of radiometer scenes of the NOAA-N satellites (of order 1 km). PIXPO 4M has the capability for 100 m accuracy, assuming suitable elements. PIXPOSC is tailored for inverse referencing with close state vectors (such as for ERS-1) and its precision is relevant to their accuracy.

Acknowledgements—We thank Dr L. Sehnal, (Astronomical Institute, Ondřejov) for providing software (density atmospheric model) for test purposes, Dr. C. A. Wagner (NOAA, Rockville) and his colleagues for information on the TBUS elements, Dr H. F. Massmann and Dr P. Schwintzer (DGFI/D-PAF, Munich and Oberpfaffenhofen) for samples of ERS-1 state vectors, and Professor Dr H. G. Wenzel (TU Karlsruhe) for his GEOPOT software. Our thanks are also due to Mrs B. Zinecker (MPIfM) for careful typing and Mrs M. Grunert (MPIfM) for drafting the figures. J. Klokočník and J. Kostelecký wish to thank MPIfM, Hamburg, for the opportunity to stay (repeatedly) at the Institute and for the support of staff during the research.

REFERENCES

1. D. Ho and A. Asem, NOAA AVHRR image referencing. *Int. J. Remote Sens.* **7,** 895 (1986).
2. W. J. Emery, J. Brown and Z. P. Nowak, AVHRR image navigation: summary and review. *Photogram. Engng Remote Sens.* **55,** 1175 (1989).
3. A. Milani, A. M. Nobili and P. Farinela, *Non-gravitational Perturbations and Satellite Geodesy*. Hilger, Bristol (1987).
4. Ch. Reigber, Lecture notes on gravity field recovery from satellite tracking data. International Summer School of Theoretical Geodesy, Assisi, Italy (1988).
5. P. Lála, A computer program for computation of ephemerides of artificial Earth satellites. *Bull. ITCP*, Washington, D.C. (1968).
6. P. Lála, Computer program PRIOR used for orbit determination at the Ondřejov Observatory. *Adv. Space Res.* **1,** 57 (1981).
7. J. Klokočník, P. Schlüssel, J. Kostelecký and H. Grassl, On the navigation of polar orbiting meteorological satellites. Max-Planck-Institut für Meteorologie, Report **75,** Hamburg (1991).
8. J. Kostelecký, EPHEM 5—an improved version of a program for satellite ephemerides. Documentation at Research Institute for Geodesy, Zdiby (1990). Program for PC.
9. G. Veis, Geodetic uses of artificial satellites. Smiths. Contribution to Astrophysics, **3,** (9), Washington, D.C. (1960).
10. ESA, Announcement of opportunity for ERS-1, technical annex: ERS-1 system description (1986).
11. P. Vass and M. Handoll, UK ERS-1 reference manual. Earth Observation Sciences, Branksome Chambers, Document DC-MA-EOS-ED-0001, Farnborough (1991).
12. C. A. Lundquist and G. Veis (Eds), *Geodetic Parameters for a 1966 Smithsonian Institution Standard Earth*, Vol. I. SAO Special Report 200, Cambridge, Mass. (1966).
13. W. M. Kaula, *Theory of Satellite Geodesy*. Blaisdell, Waltham (1966).
14. D. D. McCarthy (Ed.), *IERS Standards 1989*. IERS Technical Note 3, Observatoire de Paris (1989).
15. C. C. Goad, An efficient algorithm for the evaluation of inclination and eccentricity functions. *Manuscr. Geod.* **12,** 11 (1987).
16. J. Kostelecký, J. Klokočník and Z. Kalina, Computation of normalized inclination function to high degree for satellites in resonances. *Manuscr. Geod.* **11,** 293 (1986).
17. N. V. Emeljanov and A. A. Kanter, A method to compute inclination functions and their derivatives. *Manuscr. Geod.* **14,** 77 (1989).
18. N. J. Sneeuw, Inclination functions. TU Delft, Faculty of Geodet. Engineering, Report 91.2, Delft (1991).
19. J. Klokočník and L. Pospíšilová, Bank of Earth gravity field models in Astronomical Institute of ČSAV. Technical Report 112, Ondřejov Observatory (1991).
20. J. G. Marsh *et al.*, The GEM-T2 gravitational model. NASA Technical Memoranda 100746, Greeneblt, Md (1989).
21. P. Schwintzer *et al.*, A new Earth gravity field model in support of ERS-1 and SPOT-2: GRIM 4-S1/C1. Final report to German Space Agency DARA and French Space Agency CNES, Munich/Toulouse (1991).
22. H. G. Wenzel, GEOPOT software. Karlsruhe, private communication (1991).
23. J. Klokočník and J. Kostelecký, Earth gravity field and high satellite orbits. *Bull. Astron. Inst. Czech.* **38,** 334 (1987).
24. J. Straka, J. Klokočník and H. Grassl, Navigation of satellite measurements without ground control points. *Int. J. Remote Sens.* **14,** 1981 (1993).
25. K. F. Wakker, B. A. C. Ambrosius, R. C. A. Zandbergen and G. H. M. van Geldorp, Precise orbit computation, gravity model adjustment and altimeter data processing for the ERS-1 altimetry mission. TU Delft, Faculty of Aerospace Engineering, ESA Contract Report, Delft (1987).
26. Ch. Reigber, J. Klokočník, H. Li and F. Flechtner, Orbit dossier. German PAF for ERS-1, ERS-1 Orbit Cycles, DGFI Abt. 1, Munich, Technical Report (1988).
27. D. Brouwer, Solution of the problem of artificial satellite theory without drag. *Astron. J.* **64,** 378 (1959).
28. Y. Kozai, The motion of a close Earth satellite. *Astron. J.* **64,** 367 (1959).
29. J. Kostelecký, Ch. Reigber, J. Klokočník and J. C. Raimondo, Error assessment of the first-order perturbation theory for deep resonant cases. *Bull. Astron. Inst. Czech.* **40,** 321 (1989).
30. NASA, Format explanation of the NASA prediction bulletin. Operation Center Branch, GSFC, Greenbelt, Md (1974).
31. L. Sehnal and L. Pospíšilová, TD 88 thermosphere model. Preprint of the Astronomical Institute of Czechoslovakia, No. 67, Ondřejov (1988).
32. L. Sehnal, Second-order theory of atmospheric drag effect. In *Space Dynamics*, pp. 35–38, CEPA-DUES-Edition, CNES, Toulouse, France (1990).
33. NOAA/NESS, NOAA-telemetry revision No. 1. TBUS elements description. NOAA Report (1981).
34. J. O. Cappellari (Ed.), *Mathematical Theory of the Goddard Trajectory Determination System*, NASA GSFC X-582-76-77 report, Greenbelt, Md (1976).
35. R. H. Gooding, A second order satellite theory, with compact results in cylindrical coordinates. *Phil. Trans. R. Soc. A* **299,** 425 (1981).
36. R. H. Gooding, On mean elements for satellite orbits perturbed by the zonal harmonics of the geopotential. *Adv. Space Res.* **10,** 279 (1990).
37. R. H. Gooding, Perturbations, untruncated in eccentricity, for an orbit in an axi-symmetric gravitational field. *J. Astronaut. Sci.* **39,** 65 (1991).
38. R. H. Gooding and R. J. Taylor, A PROP 3 user's manual. RAE Technical Report 68299, Farnborough (1968).
39. J. R. Wertz (Ed.), Spacecraft attitude determination and control. Technical Staff (Attitude Systems Operation), Computer Sciences Corporation, *Reidel's Series on Astrophysics and Space Science Library*, Vol. 73. Reidel, Dordrecht (1978).